Sensors and Actuators B 229 (2016) 453–460

Contents lists available at ScienceDirect

Sensors and Actuators B: Chemical

journal homepage: www.elsevier.com/locate/snb

Effect of mesoporous structure on $Bi_{3.25}La_{0.75}Ti_3O_{12}$ powder for humidity sensing properties

Yong Zhang[a,*], Mengjiao Yuan[a], Bin Jiang[a], Peiwen Li[a], Xuejun Zheng[b]

[a] School of Physics and Optoelectronics, Xiangtan University, Xiangtan 411105, PR China
[b] School of Mechanical Engineering, Xiangtan University, Xiangtan 411105, PR China

ARTICLE INFO

Article history:
Received 27 September 2015
Received in revised form
14 December 2015
Accepted 6 February 2016
Available online 8 February 2016

Keywords:
Mesoporous structure
$Bi_{3.25}La_{0.75}Ti_3O_{12}$ powder
Humidity sensing properties
Nanocasting method
Large specific surface area

ABSTRACT

$Bi_{3.25}La_{0.75}Ti_3O_{12}$ (BLT) powder is synthesized via a metal-organic decomposition (MOD) method, and mesoporous structure is formed in the BLT powder via nanocasting method. The humidity sensing properties of BLT and mesoporous BLT (M-BLT) humidity sensors are investigated at room temperature within the relative humidity (RH) range of 11–95%. The BET surface area of M-BLT powder (10.8 m^2/g) is remarkably bigger than it of BLT powder (0.4 m^2/g). The optimum working frequency of BLT and M-BLT humidity sensors are 100 Hz, and the impedance variation of M-BLT humidity sensor is about six orders of magnitude within the whole humidity range from 11% to 95% RH, which is six times more than it of BLT humidity sensor (only about one order of magnitude). Linearity of the M-BLT humidity sensor is obviously better than it of the BLT humidity sensor, and its maximum linear error is only 2% at 75% RH. The response time and recovery time of M-BLT humidity sensor are about 32 s and 68 s at 100 Hz. The results indicate that mesoporous structure is beneficial for enhancing the humidity sensing properties of materials, and nanocasting method would be one of important and effective approach for preparing high-performance humidity-sensing material.

1. Introduction

Humidity sensor has attracted considerable attention due to its wide and essential application in industrial process control and environment monitoring, such as corrosion estimations in industry, moisture monitoring in highly sophisticated integrated circuits and food quality preservation [1–5]. Large specific surface area of the materials is beneficial for the sensing properties of the humidity sensor owing to the exposure of more active sites to the adsorbed water molecules as well as more defects forming on the surface [6,7]. Many methods can be used to prepare the materials with large specific surface area, such as hydrothermal method [8], electrospinning [9], nanocasting method [10,11] and so on. Among various preparation methods of materials, the nanocasting method is an efficient approach for synthesis of highly ordered crystalline materials, because the hard templates provide stable supports for high-temperature crystallization [6]. Moreover, the nanocasting method is one of the most significant strategies for synthesizing low-dimensional mesoporous materials with large specific surface area [12]. The humidity sensing materials with mesoporous structure have attracted considerable interests due to their uniform pore sizes, easy surface functionalization, tunable pore structures and large specific surface area [13,14]. Mesoporous materials with large specific surface area and abundant porosity can provide more defects formed on the surface and offer numerous channels and short diffusion paths for efficient transport of electrons and ions [15]. In addition, the pores of mesoporous materials can provide favorable diffusion accessibility for water molecules to move reversibly from ambient atmosphere to the inside of pores [16]. Therefore, the large specific surface area and abundant porosity of the mesoporous materials are quite helpful for the adsorption of water molecules and beneficial for humidity sensing properties of materials [17].

Rare earths have been immensely used to modify the humidity sensing properties of functional materials for their unique physicochemical activity [18,19]. Compared with simple metal oxide, complex metal oxide is a promising candidate for humidity sensors due to their higher chemistry stability and catalytic activity [20]. $Bi_4Ti_3O_{12}$ (BTO), a family of bismuth-layered perovskite compounds, belongs to Aurivillius phases, which consists of $(Bi_2O_2)^{2+}$ and perovskite-like $(A_{n-1}B_nO_{3n+1})^{2-}$ layers [21–23], and site substitution (ion substitution of A or B sites in BTO) is one of the important factors that can improve the humidity sensing properties of the materials [24,25]. La-doped BTO suppresses the evaporation

* Corresponding author.
E-mail address: zhangyong@xtu.edu.cn (Y. Zhang).

http://dx.doi.org/10.1016/j.snb.2016.02.022
0925-4005/

of bismuth and the extensive grain growth [26,27], and La-doping results in oxygen vacancies and crystalline structure defects, which is beneficial for the adsorption of water molecules [28]. According to previous works [29–31], there is good crystallinity for the ($Bi_{4-x}La_xTi_3O_{12}$) at a composition around $x = 0.75$, therefore it is expected that La-doping may greatly enhance the humidity sensing performance of BTO.

In this paper, $Bi_{3.25}La_{0.75}Ti_3O_{12}$ (BLT) powder is synthesized via a metal-organic decomposition (MOD) method, and mesoporous structure is formed in the BLT powder via nanocasting method by using mesoporous silica SBA-15 as the hard template. The BLT and mesoporous BLT (M-BLT) powders are characterized by X-ray diffraction (XRD), field-emission scanning electron microscopy (FE-SEM), transmission electron microscopy (TEM) and specific surface and pore size analysis instrument, which subsequently fabricated by coating them on the ceramic substrates with Ag–Pd interdigitated electrodes to form the humidity sensors. In order to investigate the effect of mesoporous structure on BLT powder, the humidity sensing properties of BLT and M-BLT humidity sensors are measured in the whole relative humidity (RH) range of 11–95%. To avoid the polarization effects of adsorbed water, the sensing properties of many ionic-type humidity sensors should be evaluated by impedance changes [32]. We expect that the results may offer useful guidelines to prepare high-performance humidity-sensing materials with large specific surface area.

2. Experiment

2.1. Preparations and characterizations of BLT and M-BLT powders

The BLT powder was synthesized by MOD method. The BLT precursor solution was prepared by mixing bismuth nitrate, lanthanum acetate and tetrabutyl titanate. Firstly, an appropriate amount of bismuth nitrate was dissolved in acetic acid and 2-methoxyethanol with a volume ratio of 1:1 in air (solution A). Meanwhile, lanthanum acetate was dissolved in acetic acid and deionized water with a volume ratio of 2:1 (solution B). Then, the solutions A and B were mixed and constantly stirred for about 2 h until a transparent solution (solution C) was obtained. Subsequently, in order to prevent the hydrolysis caused by the moisture in air, acetylacetone was added into the transparent solution C. At last, a stoichiometric amount of tetrabutyl titanate solution was added to the mixture solution. This mixture solution was left for 12 h under stirring at room temperature. The as-prepared mixture solution was carefully transferred to a dish, dried at 100 °C for three days to evaporate the solvent and then calcined at 750 °C for 3 h to obtain the yellow BLT powder.

In order to prepare M-BLT powder subsequently, the hexagonal mesoporous silica SBA-15 as hard template was prepared firstly. The detailed procedure was shown as follows: firstly, 2 g Pluronic P123 ($EO_{20}PO_{20}EO_{20}$, MW = 5800, Sigma–Aldrich) as a surfactant template was dissolved in 60 ml HCl solution (2 M) at room temperature. Then, 4.25 g tetraethyl orthosilicate (TEOS) was added dropwise under stirring at 40 °C for 24 h. Subsequently the mixture was transferred into a closed Teflon-lined stainless steel autoclave and subsequently heated at 100 °C for 24 h under a static condition. The autoclave was cooled down naturally. Finally, the product was filtered off, washed with deionized water, dried at 80 °C for 12 h, and calcined at 550 °C for 6 h to obtain the pure mesoporous silica SBA-15.

The M-BLT powder was synthesized via MOD method combining with nanocasting method, and the preparation procedure was shown as follows: firstly, 0.5 g as-prepared silica SBA-15 was added to the solution C. Acetylacetone was added into the mixture solution so as to prevent the hydrolysis caused by the moisture in air. Then, a stoichiometric amount of tetrabutyl titanate solution was added. The above mixture solution was stirred for 12 h at room temperature, dried at 100 °C, and calcined at 550 °C for 3 h to obtain the light yellow powder. To make the BLT precursor fully into the pores channel of silica SBA-15 template, the second impregnation process was shown as follows: firstly, the molar volume of bismuth nitrate, lanthanum acetate and tetrabutyl titanate in half and the above light yellow powder were mixed, then the mixture solution was repeated following the above same conditions. The resultant powder was calcined at 750 °C for 3 h to obtain BLT/SiO_2 powder. Finally, the silica SBA-15 template was removed by using NaOH aqueous solution (2 M) at room temperature for three times. The yellow M-BLT powder was obtained by washing with water and ethanol, and drying at 80 °C for 12 h.

The crystalline structures of the BLT, SBA-15 and M-BLT powders were observed by XRD (Germany, Brukers-AXS, D8 Advance) with a Cu Kα ($\lambda = 0.15418$ nm). The morphologies were characterized by using FE-SEM (Japan, Hitachi, S-4800) and TEM (Japan, JEOL, JEM-2100). The N_2 adsorption/desorption isotherm studies were performed on a specific surface and pore size analysis instrument (China, Beishide Instrument Technology (Beijing) Co., Ltd., 3H-2000PS). The specific surface area was determined from the linear part of the Brunauer–Emmett–Teller (BET) plot, and the average pore size was calculated from the desorption branch based on the Barrett–Joyner–Halenda (BJH) method.

2.2. Fabrication and measurement of the humidity sensor

The as-synthesized BLT and M-BLT powders were respectively mixed with deionized water in a weight ratio of 4:1 to form the pastes. The pastes were coated onto the substrate (6 mm × 3 mm × 0.5 mm) with five pairs of Ag–Pd interdigitated electrodes (electrodes width and distance: 0.15 mm) to form a sensing film, and then the film was dried in air at 60 °C for 5 h. Before the humidity sensing test, all the humidity sensors were aged with a voltage AC 1 V for 24 h under 95% RH vapor environment [7,33]. The schematic diagrams of the humidity sensor structure and the measurement setup are shown in Fig. 1.

The humidity sensing properties of the BLT and M-BLT humidity sensors were measured on intelligent humidity sensitive analysis system (China, Beijing Elite Technology Co., Ltd., CHS-1). The AC voltage applied was 1 V, and the frequency varied from 10 Hz to 100 kHz. The controlled humidity environment was achieved by supersaturated aqueous solutions of LiCl, $MgCl_2$, $Mg(NO_3)_2$, NaCl, KCl, and KNO_3 in a closed glass vessel at room temperature, which yielded approximately 11%, 33%, 54%, 75%, 85% and 95% RH, respectively [34]. 10 h were spent to ensure the air in the glass vessel reaches equilibrium state in the investigations. The RH of laboratory atmosphere was maintained at 25% RH by using an automatic drier. The response time and recovery time were defined as the time taken by a sensor to achieve 90% of the total impedance change in the case of adsorption and desorption [35,36]. The hysteresis was measured by switching the humidity sensor between the chambers of 11%, 33%, 54%, 75%, 85% and 95% RH, and then shifting back. All of the sensing measurements were performed at a constant temperature of 25 °C.

3. Results and discussion

3.1. Materials characterization

Fig. 2(a) shows the low-angle XRD patterns of SBA-15, BLT and M-BLT powders. There are three diffraction peaks in the low-angle XRD pattern of SBA-15, which can be indexed to the (1 0 0), (1 1 0)

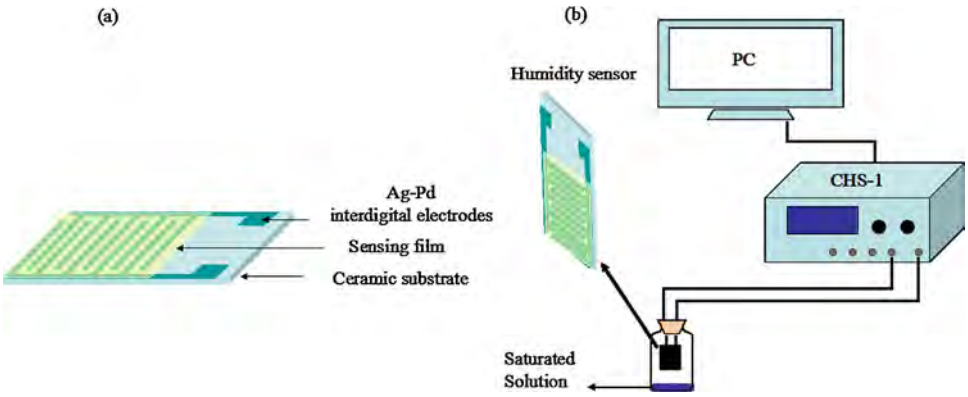

Fig. 1. The schematic diagrams of (a) the humidity sensor structure and (b) the measurement setup.

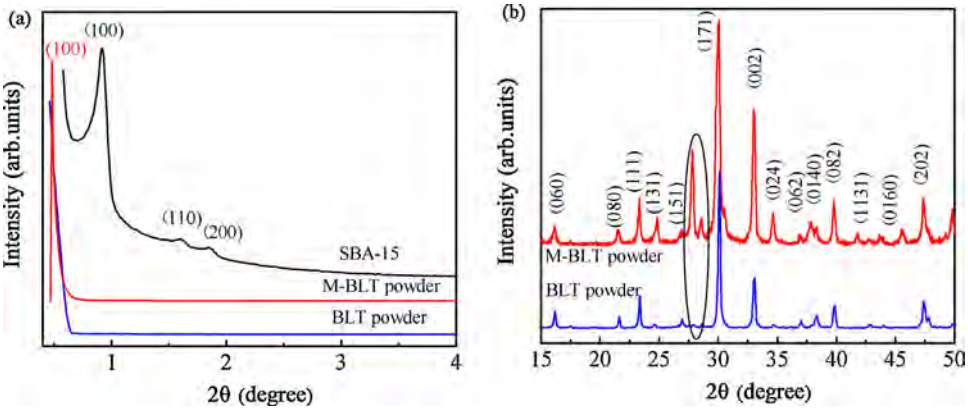

Fig. 2. (a) Low-angle XRD patterns of SBA-15, BLT and M-BLT powders; (b) Wide-angle XRD patterns of BLT and M-BLT powders.

and (2 0 0) reflections of two-dimensional hexagonal mesoporous structure [37]. The (1 0 0) diffraction peak also appears in the low-angle XRD pattern of M-BLT powder but not be observed in the low-angle XRD pattern of BLT powder. From Fig. 2(a), the (1 0 0) diffraction peak of M-BLT powder is shifted to the lower angles compared to that of SBA-15. According to previous work [6,7], the appearance of (1 0 0) diffraction peak illustrates that the M-BLT powder is of mesoporous structure which is replicated from SBA-15 template. Compared with the template SBA-15, the (1 1 0) and (2 0 0) diffraction peaks cannot be observed in the low-angle XRD pattern of M-BLT powder, and this is due to the BLT precursor incompletely filling into the SBA-15 template pores [7], which illustrates the ordering of the pore array is decreased [38,39]. Moreover, because the radiuses of Bi and La atoms are bigger than Si atomic radius of SBA-15, the interplanar distance of the M-BLT powder with the SBA-15 template removed is bigger than it of the SBA-15 powder [40], resulting in the diffraction peaks of M-BLT powder shifting to the lower angles compared with that of SBA-15. The above discussions show that the mesoporous structure which is similar to the SBA-15 template is replicated to the M-BLT powder while not formed in the BLT powder. The wide-angle XRD patterns of BLT and M-BLT powders are shown in Fig. 2(b). It can be noted that the diffraction peaks of BLT and M-BLT powders can be indexed to the orthorhombic BTO (ICSD #240210) [41], and BLT and M-BLT powders exhibit a perovskite phase. From the figure, the diffraction peak of SBA-15 at $2\theta = 28.6^{\circ}$ is observed in the M-BLT powder while not observed in the BLT powder, and this phenomenon is caused by the residual Si of the M-BLT from the SBA-15 template [6,7]. In addition, all diffraction peaks of M-BLT powder are more intensive than these of BLT powder, which indicates that the obtained perovskite-type M-BLT powder is of better crystal quality [42,43].

The morphologies of BLT and M-BLT powders are characterized by FE-SEM and shown in Fig. 3(a) and (b). It can be clearly seen from Fig. 3(a) that the BLT powder is composed of the irregular grains with size of about 200 nm and formed a dense structure. From Fig. 3(b), M-BLT powder is of fluffy microstructure and is featured by a high porosity. Compared with BLT powder with dense structure, the M-BLT powder with fluffy microstructure may be of larger specific surface area, which may be quite helpful for the water molecules adsorption and beneficial for its humidity sensing properties [44,45]. To further investigate the morphologies of the BLT and M-BLT powders, the TEM images of the BLT and M-BLT powders are performed as shown in Fig. 3(c) and (d). It can be seen from Fig. 3(c) that the BLT powder is of dense and nonporous microstructure. From the inset of Fig. 3(c), it is obviously that the BLT powder is composed of many crystallites and formed a dense structure, which is consistent with the FE-SEM image mentioned above. From Fig. 3(d), the abundant mesoporous can be found in M-BLT powder and the pore diameter is about 20 nm, which may be quite helpful for the adsorption of water molecules and is in good agreement with the FE-SEM image. From the above discussions, the introduction of mesoporous structure makes the M-BLT powder have a fluffy microstructure, which may be quite helpful for the adsorption of water molecules.

The N_2 adsorption–desorption isotherms and the corresponding pore size distribution of the BLT and M-BLT powders are shown in Fig. 4. As seen in Fig. 4(a), the N_2 adsorption–desorption isotherm of BLT powder is identified as type III isotherm, and it shows that the BLT powder is of mesoporous and macroporous [46]. From the figure, two hysteresis loops appear in the relative pressure ranges from 0.4–0.85 and 0.85–1.0 (P/P_0). The formation of first loop at 0.4–0.85 is due to capillary condensation within mesoporous, and

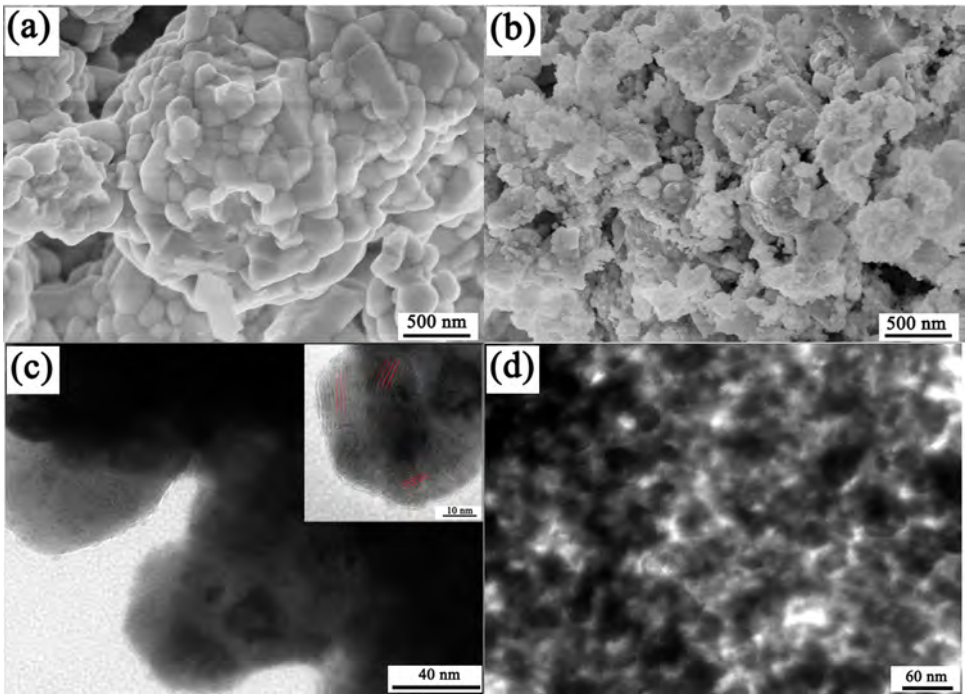

Fig. 3. FE-SEM images of (a) BLT and (b) M-BLT powders; (c) TEM images of BLT powder and (d) M-BLT powder.

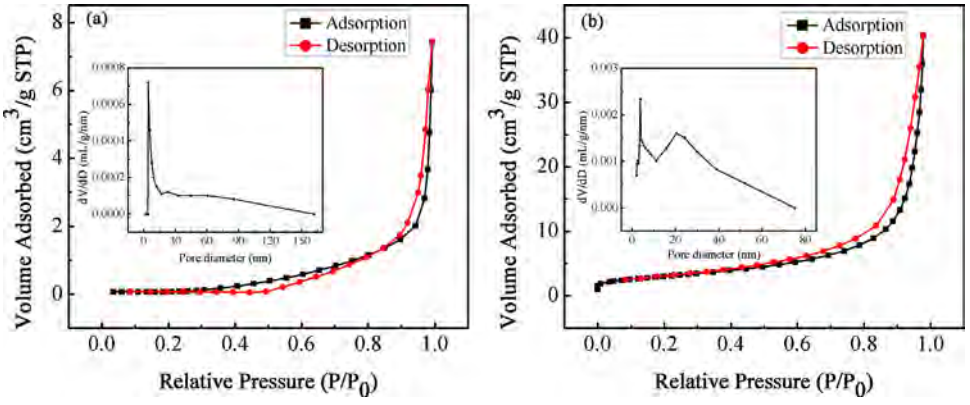

Fig. 4. Nitrogen adsorption-desorption isotherms and the corresponding pore size distribution of (a) BLT powder and (b) M-BLT powder.

the second loop may arise from macropore [47]. The inset in Fig. 4(a) is the pore diameter distribution of the BLT powder. The ranges of pore diameters for BLT powder are from 2 to 161 nm and the average pore size of the BLT powder is 121 nm, this indicates BLT powder is mainly composed of macropore. It can be seen from Fig. 4(b) that the N_2 adsorption–desorption isotherm of M-BLT powder presents the typical type-IV isotherm with a H3 hysteresis loop in the relative pressure range of 0.6–1.0, indicating that the M-BLT powder is mainly composed of mesoporous [15,48], which is further verified by the BJH pore size distribution data shown in the inset of Fig. 4(b). The M-BLT powder is of a pore size distribution from 2 to 60 nm and the average pore size of the M-BLT powder is 23.2 nm, which indicates M-BLT powder is of mesoporous structure and it is consistent with the results of low-angle XRD, FE-SEM and TEM images. In addition, the BET surface area, pore volume and pore size distribution of BLT and M-BLT powders are given in Table 1. As shown in Table 1, the BET surface area and pore volume of M-BLT powder (10.8 m^2/g and 0.063 cm^3/g) are remarkably higher than those of BLT powder (0.4 m^2/g and 0.012 cm^3/g). Because the large specific surface area and pore volume of the mesoporous materials are quite helpful for the adsorption of water molecules, the formation of mesoporous structure in humidity sensing materials can greatly improve humidity sensing properties [13–15]. The results illustrate that the M-BLT powder is of better humidity sensing performance than BLT powder.

Table 1
The textural properties of BLT powder and M-BLT powder.

Sample	BET surface area (m^2/g)	Pore volume (cm^3/g)	Average pore size (nm)
BLT powder	0.4	0.012	121
M-BLT powder	10.8	0.063	23.2

3.2. Humidity sensing properties

Fig. 5 shows the dependence of impedance on RH for BLT and M-BLT humidity sensors at different frequencies. From Fig. 5(a) and (b), the impedance of BLT and M-BLT humidity sensors is both found to decrease with the frequency increasing, and their optimum working frequency are both 100 Hz. Furthermore, when the

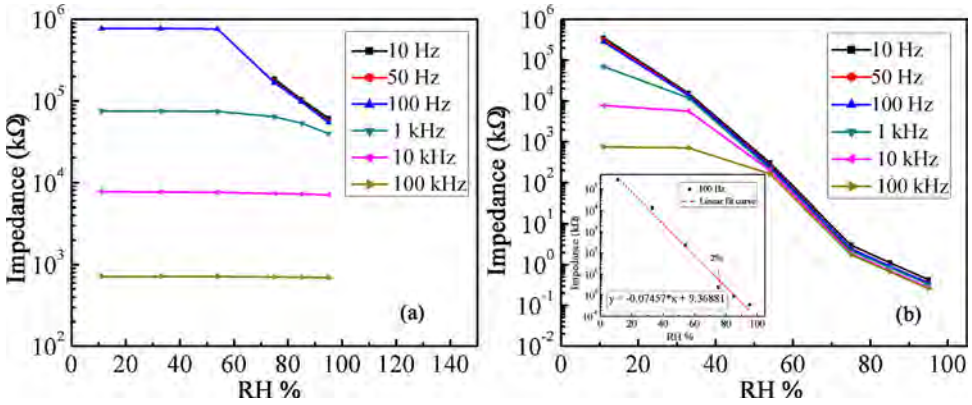

Fig. 5. Impedance vs. RH curves of (a) BLT and (b) M-BLT humidity sensors at various frequencies. Insert shows the calibration curve of M-BLT humidity sensor in the range of 11–95% RH at 100 Hz.

frequency is 100 Hz, it can be clearly seen that the impedance variation of the BLT humidity sensor (only about one order of magnitude) is obviously smaller than it of the M-BLT humidity sensor (about six orders of magnitude) within the whole humidity range from 11% to 95% RH, which illustrates that the impedance of BLT humidity sensor changes a little and the BLT humidity sensor is of low sensitivity. It should be noted that there is no data for 11, 33 and 54% RH at 10 and 50 Hz in Fig. 5(a), which is because the impedance value of BLT humidity sensor is too large (over 10^9 Ω), and the humidity sensing materials with the high impedance are unsuitable for fabricating the humidity sensors [49,50]. As shown in Fig. 5(b), at low RH, the impedance curves turn flat at high frequency, which indicates that the impedance of the M-BLT humidity sensor becomes independent of RH. This is because the electrical field direction changes fast at high frequencies and the polarization of water cannot catch up with it, resulting in the capacitance and the dielectric constant of the M-BLT humidity sensor being small and independent of the RH [51,52]. Therefore, mesoporous structure of materials is beneficial for enhancing the humidity sensing properties. The linearity error is traditionally defined as the maximum deviation from a linear fit (before or after a calibration procedure), expressed in percent of the full range [53]. The inset of Fig. 5(b) shows the calibration curve of M-BLT humidity sensor in the range of 11–95% RH at 100 Hz. As can be seen from the inset of Fig. 5(b), the absolute value of the slope is defined as the sensitivity of the humidity sensor, and its maximum linear error is only 2% at 75% RH. When the frequency is 100 Hz, M-BLT humidity sensor is of good linearity and high humidity sensitivity in the whole RH range. It is worth mentioning from Fig. 5(b) that the M-BLT humidity sensor also has good linearity and high humidity sensitivity when the frequencies are 10 Hz and 50 Hz, and their maximum linear errors are 2% at 75% RH, which means that the M-BLT humidity sensor may be of low operating frequencies and the working frequency range of it is broadened. The operating frequency of 100 Hz for M-BLT humidity sensor is applied in all investigations hereinafter.

It is well known that response and recovery behaviors are the important characteristic parameter for evaluating the performance of the humidity sensor. Fig. 6(a) shows the response and recovery properties of the M-BLT humidity sensor corresponding to several continuous water adsorption and desorption processes by switching the measurement atmosphere between 11% and 95% RH. As can be seen from the figure, the M-BLT humidity sensor shows good repeatability in the continuous measurements. At the operating frequencies of 100 Hz, the response time (as the humidity changes from 11 to 95% RH) is approximately 32 s and the recovery time (as the humidity changes from 95 to 11% RH) is about 68 s. The recovery time is longer than response time, which is due to the slow desorption rate of water molecules among the M-BLT powder. Although the M-BLT humidity sensor is inevitably exposed to the laboratory atmosphere (about 25% RH) during the switching process, the switching time (about 1–2 s) is smaller than the response time (32 s) of the M-BLT humidity sensor. Therefore, the correctness of this experiment is acceptable, and it is consistent with the previous experiments [54–56].

Hysteresis is one of the most important characteristic parameters which is usually used to estimate the reliability of humidity sensors [57], and it is defined as the maximum difference between the two outputs (adsorption and desorption cycle). Fig. 6(b) shows the humidity hysteresis properties of the M-BLT humidity sensor at 100 Hz. It can be seen that the impedance changes from about 10^8 to 10^3 Ω when RH changes from 11% to 95%. The upper line in the figure stands for the course from low to high RH corresponding to the adsorption process, while the other stands for the desorption process. Moreover, the insets of Fig. 6(b) show the humidity hysteresis properties of the M-BLT humidity sensor at 10 and 50 Hz. At 10, 50 and 100 Hz, the maximum humidity hystereses of the M-BLT humidity sensor are 12.7%, 13.3% and 12.0% RH respectively, which illustrates that the M-BLT humidity sensor is of the best reliability at the operating frequency of 100 Hz [45,57].

3.3. Discussion on the humidity sensing mechanism

The complex impedance plots can be used to research the humidity sensing behaviors of materials [17,48]. The complex impedance plots of the M-BLT humidity sensor at different RH are shown in Fig. 7. The impedance measurements are made at frequencies from 10 Hz to 100 kHz with a testing voltage of 1 V. Here, ReZ and ImZ are the real part and imaginary part of the complex impedance. As can be seen from Fig. 7(a), when the RH is low (11% RH), a semicircle is observed, and the semicircle of the complex impedance plot represents a kind of conduction mechanism which can be modeled as an equivalent parallel circuit that incorporates a resistor and a capacitor [53]. According to the protons conductivity model of Anderson and Parks [58], when the RH is low, only a few water molecules are adsorbed, and the coverage of water on the surface of sensing material is not continuous and proton migrates only by hopping from site to site across the M-BLT powder surface, resulting in high impedance of the M-BLT humidity sensor. In Fig. 7(b) and (c), with an increase of humidity (33%, 54% RH), the semicircle radius gradually decreases and a straight line appears at low frequencies, and the higher the RH is, the longer the line is. The line represents Warburg impedance due to the diffusion of the electroactive species at the electrode [59,60]. Under this condition, with increase of adsorbing water molecules, the surface water layers of M-BLT powder are close to liquid water. According to the Grotthuss chain mechanism [61], $H_2O + H_3O^+ \rightarrow H_3O^+ + H_2O$,

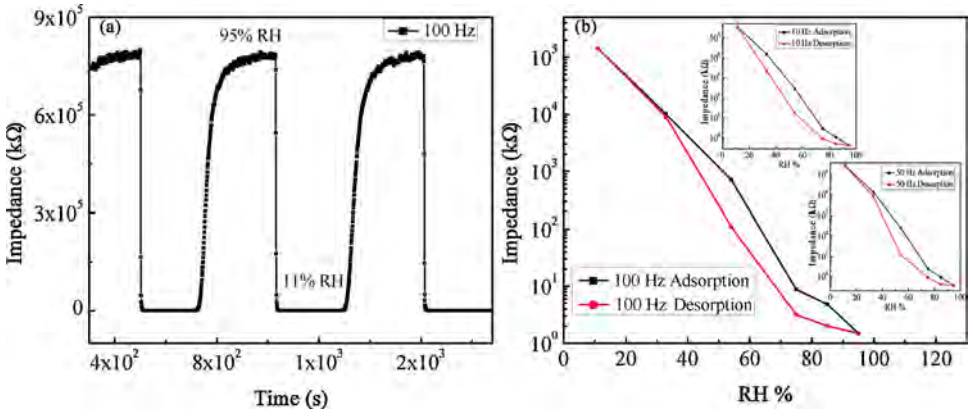

Fig. 6. (a) Transient response characteristics and (b) Humidity hysteresis characteristic of the M-BLT humidity sensor at 100 Hz. Inserts show the humidity hysteresis characteristics of the M-BLT humidity sensor at 10 and 50 Hz.

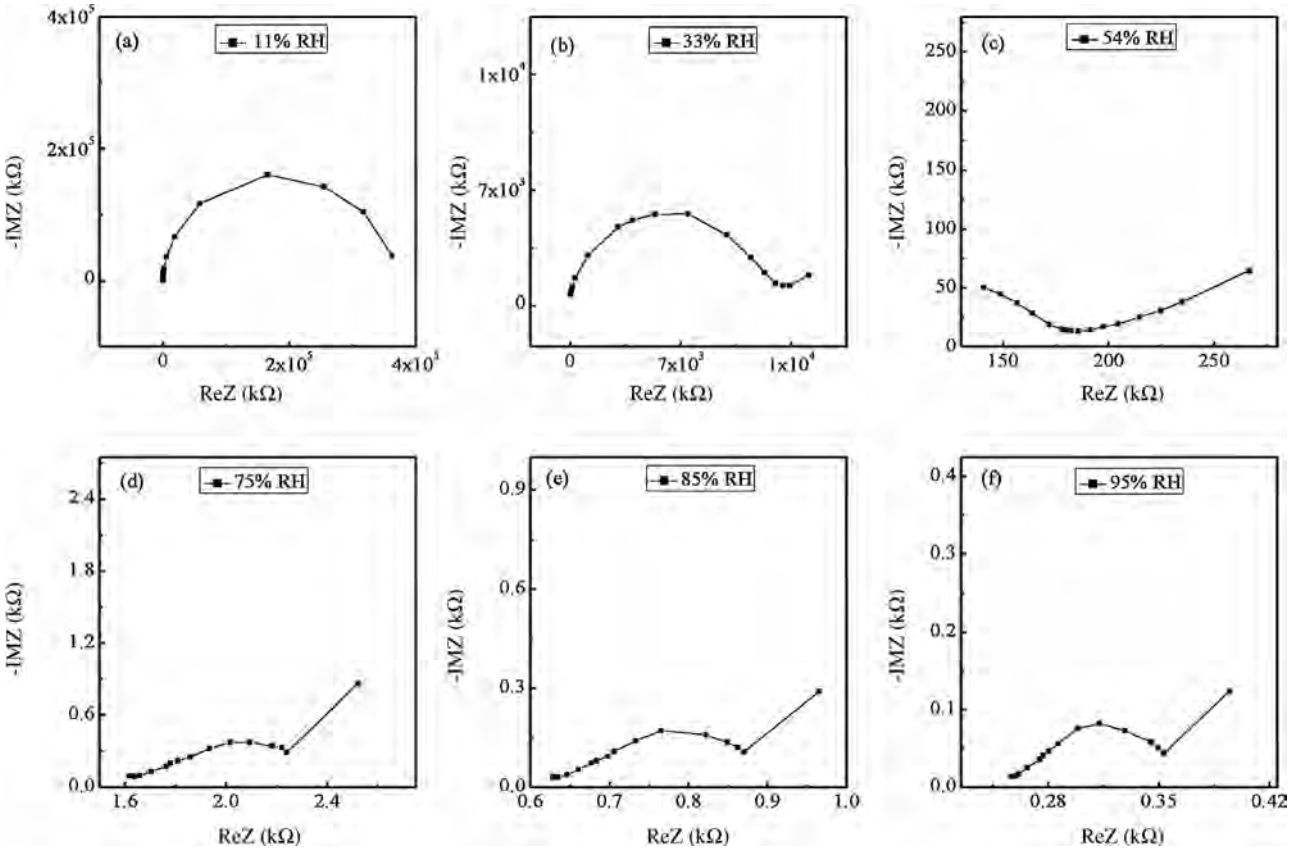

Fig. 7. The complex impedance plots of the M-BLT humidity sensor measured at (a) 11%, (b) 33%, (c) 54%, (d) 75%, (e) 85%, and (f) 95% RH in the frequency range from 10 Hz to 100 kHz.

the initial and final states are the same, and the energy is also equivalent, so that the transfer of H_3O^+ is quite easy. On the other hand, according to the model of ion transport mechanism reported by Casalbore-Miceli et al. [62], a few of La^+ ions could be dissociated into free ions and the impedance of the sensing film decreases sharply [63,64]. In Fig. 7(d)–(f), further along with increasing RH (75%, 85% and 95% RH), the first semicircle disappears, and the second semicircle with a straight line is observed. The disappearance of first semicircle indicates that more and more La^+ ions from the dissolved M-BLT surface dissociate into free ions with the RH increasing, and the active electrolytic conduction takes place in the adsorbed layers of materials surface [43,45]. In addition, the water molecules are not only adsorbed on the outer surface of M-BLT but also entered into the pore and then adsorbed on the pore walls [65]. The pore (about 23.2 nm) will be beneficial for diffusion of water molecules, therefore enhancing the high rate transport of water molecules throughout the humidity sensor. At high RH, the liquid water is condensed into the mesoporous [66] and one or several serial water layers are formed in the pore walls surface, thus protonic transport takes place in the adsorbed layers of the pore walls surface subsequently in addition to the active electrolytic conduction in the adsorbed layers of materials surface. On the other hand, the surface defects and oxygen vacancies are generated gradually due to the dissociation of La^+ ions in the dissolved M-BLT surface, resulting in an increase of adsorption sites for water molecules [45], and the second semicircle with a straight line is observed in

the complex impedance plots. Therefore, with the RH increasing, the impedance of M-BLT powder continuously decreases about six orders of magnitude comparing with the initial value.

4. Conclusion

In conclusion, the BLT powder is synthesized via a MOD method, and mesoporous structure is formed in the BLT powder via nanocasting method by using mesoporous silica SBA-15 as the hard template. Benefiting from the mesoporous structures with large specific surface area and abundant porosity, the humidity sensor based on M-BLT powder is of superior humidity performance compared with BLT humidity sensor. The optimum working frequency of the M-BLT and BLT humidity sensors is 100 Hz, and the impedance variation of the M-BLT humidity sensor is about six orders of magnitude within the whole humidity range from 11% to 95% RH, which is six times more than it of the BLT humidity sensor (only about one order of magnitude). Furthermore, the M-BLT humidity sensor is of low operating frequency and wide working frequency range, and the response time and recovery time of M-BLT humidity sensor are about 32 s and 68 s at 100 Hz. The results indicate that the mesoporous structure is useful for improving the humidity sensitivity of materials, and nanocasting method would be one of important and effective approach for preparing high-performance humidity-sensing materials with large specific surface area.

Acknowledgements

This work was supported by NNSF of China (51402250, 51272158), Hunan Provincial Natural Science Foundation of China (2015JJ4046, 14JJ6040) and Scientific Research Fund of Hunan Provincial Education Department (14B168).

References

[1] A.E. Dessler, S.C. Sherwood, A matter of humidity, Science 323 (2009) 1020–1021.
[2] X.F. Wang, B. Ding, J.Y. Yu, M. Wang, F.K. Pan, A highly sensitive humidity sensor based on a nanofibrous membrane coated quartz crystal microbalance, Nanotechnology 21 (2010) 055502.
[3] Z. Zhang, C. Hu, Y. Xiong, R. Yang, Z. Wang, Synthesis of Ba-doped CeO_2 nanowires and their application as humidity sensors, Nanotechnology 18 (2007) 465504.
[4] A. Kolmakov, D.O. Klenov, Y. Lilach, S. Stemmer, M. Moskovits, Enhanced gas sensing by individual SnO_2 nanowires and nanobelts functionalized with Pd catalyst particles, Nano Lett. 5 (2005) 667–673.
[5] H.N. Zhang, Z.Y. Li, L. Liu, C. Wang, Y. Wei, A.G. MacDiarmid, Mg^{2+}/Na^{+}-doped rutile TiO_2 nanofiber mats for high-speed and anti-fogged humidity sensors, Talanta 79 (2009) 953–958.
[6] Y.G. Wang, J.W. Ren, Y.Q. Wang, F.Y. Zhang, X.H. Liu, Y. Guo, G.Z. Lu, Nanocasted synthesis of mesoporous $LaCoO_3$ perovskite with extremely high surface area and excellent activity in methane combustion, J. Phys. Chem. C 112 (2008) 15293–15298.
[7] J. Zhao, Y.P. Liu, X.W. Li, G.Y. Lu, L. You, X.S. Liang, F.M. Liu, T. Zhang, Y. Du, Highly sensitive humidity sensor based on high surface area mesoporous $LaFeO_3$ prepared by a nanocasting route, Sens. Actuators B 181 (2013) 802–809.
[8] Y. Chen, Y.P. Zhang, D.M. Li, F.L. Gao, C.H. Feng, S.P. Wen, S.P. Ruan, Humidity sensor based on $AlPO_4$-5 zeolite with high responsivity andits sensing mechanism, Sens. Actuators B 212 (2015) 242–247.
[9] D. Li, Y.N. Xia, Fabrication of titania nanofibers by electrospinning, Nano Lett. 3 (2003) 555–560.
[10] D. Shu, H.H. Cheng, C.J. Lv, M.A. Asi, L. Long, C. He, X.P. Zou, Z.X. Kang, Soft-template synthesis of vanadium oxynitride–carbon nanomaterials for supercapacitors, Int. J. Hydrogen Energy 39 (2014) 16139–16150.
[11] C. Deeprasertkul, R. Longloilert, T. Chaisuwan, S. Wongkasemjit, Impressive low reduction temperature of synthesized mesoporous ceria via nanocasting, Mater. Lett. 130 (2014) 218–222.
[12] A. Bearzotti, J.M. Bertolo, P. Innocenzi, P. Falcaro, E. Traversa, Humidity sensors based on mesoporous silica thin films synthesised by block copolymers, J. Eur. Ceram. Soc. 24 (2004) 1969–1972.
[13] X.H. Sun, Y.F. Shi, P. Zhang, C.M. Zheng, X.Y. Zheng, F. Zhang, Y.C. Zhang, N.J. Guan, D.Y. Zhao, G.D. Stucky, Container effect in nanocasting synthesis of mesoporous metal oxides, J. Am. Chem. Soc. 133 (2011) 14542–14545.
[14] J.C. Tu, R. Wang, W.C. Geng, X.Y. Lai, T. Zhang, N. Li, N.L. Yue, X.T. Li, Humidity sensitive property of Li-doped 3D periodic mesoporous silica SBA-16, Sens. Actuators B 136 (2009) 392–398.
[15] Y.R. Zhu, Z.B. Wu, M.J. Jing, W.X. Song, H.S. Hou, X.M. Yang, Q.Y. Chen, X.B. Ji, 3D network-like mesoporous $NiCo_2O_4$ nanostructures as advanced electrode material for supercapacitors, Electrochim. Acta 149 (2014) 144–151.
[16] T. Zhang, R. Wang, W.C. Geng, X.T. Li, Q. Qi, Y. He, S.J. Wang, Study on humidity sensing properties based on composite materials of Li-doped mesoporous silica A-SBA-15, Sens. Actuators B 128 (2008) 482–487.
[17] T. Fei, K. Jiang, S. Liu, T. Zhang, Humidity sensors based on Li-loaded nanoporous polymers, Sens. Actuators B 190 (2014) 523–528.
[18] M. Anbia, S.E.M. Fard, Improving humidity sensing properties of nanoporous TiO_2–10 mol% SnO_2 thin film by co-doping with La^{3+} and K^{+}, Sens. Actuators B 160 (2011) 215–221.
[19] H.X. Li, Z.M. Shi, H.W. Liu, Humidity sensing properties of La^{3+}/Ce^{3+}-doped TiO_2–20 wt.% SnO_2 thin films derived from sol–gel method, J. Rare Earths 28 (2010) 123–128.
[20] M.C. Zhang, C.G. Hu, H. Liu, Y.F. Xiong, Z.W. Zhang, A rapid-response humidity sensor based on $BaNbO_3$ nanocrystals, Sens. Actuators B 136 (2009) 128–132.
[21] B.H. Park, S.J. Hyun, C.R. Moon, B.D. Choe, J. Lee, C.Y. Kim, W. Jo, T.W. Noh, Imprint failures and asymmetric electrical roperties induced thermal processes in epitaxial $Bi_4Ti_3O_{12}$ thin film, J. Appl. Phys. 84 (1998) 4428.
[22] M. Yamaguchi, T. Nagatomo, preparation and properties of $Bi_4Ti_3O_{12}$ thin films grown at low substrate temperatures, Thin Solid Films 348 (1999) 294–298.
[23] K.T. Kim, Chang-Il Kim, Characterization of ferroelectric $Bi_{3.25}La_{0.75}Ti_3O_{12}$ thin films prepared by metal organic decomposition method, Thin Solid Films 478 (2005) 6–12.
[24] S.K. Singh, H. Ishiwara, Ferroelectric properties enhancement in niobium-substituted $Bi_{3.25}La_{0.75}Ti_3O_{12}$ thin films prepared by chemical solution route, Thin Solid Films 497 (2006) 90–95.
[25] T. Watanabe, T. Kojima, T. Sakai, H. Funakubo, M. Osada, Y. Noguchi, M. Miyayama, Large remanent polarization of $Bi_4Ti_3O_{12}$-based thin films modified by the site engineering technique, J. Appl. Phys. 92 (2002) 1518.
[26] J.H. Park, J.S. Bae, H.J. Park, Y.S. Kim, B.E. Jun, B.C. Choi, J.H. Jeong, Electric response as a function of applied voltage of Nb-doped $Bi_4Ti_3O_{12}$ thin films, Thin Solid Films 516 (2008) 5304–5308.
[27] N. Zhong, T. Shiosaki, C-axis-oriented $Bi_{3.25}La_{0.75}Ti_3O_{12}$ ferroelectric thin film fabricated by chemical solution deposition, Mater. Lett. 61 (2007) 2935–2938.
[28] P. Gautam, A. Sachdeva, S.K. Singh, R.P. Tandon, Dielectric functions and energy band gap variation studies of manganese doped $Bi_{3.25}La_{0.75}Ti_3O_{12}$ thin films using spectroscopic ellipsometry, J. Alloys Compd. 617 (2014) 374–378.
[29] F. Yakuphanoglu, A. Tataroğlu, A.A. Al-Ghamdi, R.K. Gupta, Y. Al-Turki, Z. Şerbetçi, S.B. Omran, F. El-Tantawy, Ferroelectric $Bi_{3.25}La_{0.75}Ti_3O_{12}$ photodiode for solar cell applications, Sol. Energy Mater. Sol. Cells 133 (2015) 69–75.
[30] S.H. Hu, J. Chen, Z.G. Hu, G.S. Wang, X.J. Meng, J.H. Chu, N. Dai, The optical properties of $Bi_{3.25}La_{0.75}Ti_3O_{12}$ thin films with different thickness prepared by chemical solution deposition, Mater. Res. Bull. 39 (2004) 1223–1229.
[31] G. Xu, G.R. Han, the low temperature synthesis and characterization of $Bi_{3.25}La_{0.75}Ti_3O_{12}$ powder by hydroxide coprecipitation in aqueous medium, Mater. Res. Bull. 39 (2004) 1909–1915.
[32] Y. Zhang, X.J. Zheng, T. Zhang, S.H. Dai, Y.Q. Chen, L.J. Gong, Humidity sensing properties of the sensor based on $Bi_{0.5}K_{0.5}TiO_3$ powder, Sens. Actuators B 147 (2010) 180–184.
[33] Q. Qi, T. Zhang, Y. Zeng, H.B. Yang, Humidity sensing properties of KCl-doped Cu–Zn/CuO–ZnO nanoparticles, Sens. Actuators B 137 (2009) 21–26.
[34] L. Greenspan, Humidity fixed points of binary saturated aqueous solutions, J. Res. NBS 81A (1977) 89–96.
[35] S. Agarwal, G.L. Sharma, Humidity sensing properties of (Ba, Sr)TiO_3 thin films grown by hydrothermal–electrochemical method, Sens. Actuators B 85 (2002) 205–211.
[36] J.H. Cho, J.B. Yu, J.S. Kim, S.O. Sohn, D.D. Lee, J.S. Huh, Sensing behaviors of polypyrrole sensor under humidity condition, Sens. Actuators B 108 (2005) 389–392.
[37] Z. Luan, M. Hartmann, D. Zhao, W. Zhou, L. Kevan, Alumination and ion exchange of mesoporous SBA-15 molecular sieves, Chem. Mater. 11 (1999) 1621–1627.
[38] S.V. Nguyen, V. Szabo, D. Trong On, S. Kaliaguine, Mesoporous silica supported $LaCoO_3$ perovskites as catalysts for methane oxidation, Microporous Mesoporous Mater. 54 (2002) 51–61.
[39] J. Deng, L. Zhang, H. Dai, C.T. Au, In situ hydrothermally synthesized mesoporous $LaCoO_3$/SBA-15 catalysts: high activity for the complete oxidation of toluene and ethyl acetate, Appl. Catal. A 352 (2009) 43–49.
[40] Z.F. Mu, Y.H. Hu, H.Y. Wu, C.J. Fu, F.W. Kang, The structure and luminescence properties of a novel orange emitting phosphor $Y_3Mn_xAl_{5-2x}Si_xO_{12}$, Physica B 406 (2011) 864–868.
[41] H.C. Du, L.J. Tang, S. Kaskel, Preparation Microstructure, and Ferroelectric Properties of $Bi_{3.25}La_{0.75}Ti_{3-x}M_xO_{12}$ (M = Mo, W, Nb, V), J. Phys. Chem. C 113 (2009) 1329–1339.
[42] P. Gautam, A. Sachdeva, Sushil K. Singh, R.P. Tandon, Dielectric functions and energy band gap variation studies of manganese doped $Bi_{3.25}La_{0.75}Ti_3O_{12}$ thin films using spectroscopic ellipsometry, J. Alloys Compd. 617 (2014) 374–378.
[43] M.J. Yuan, Y. Zhang, X.J. Zheng, B. Jiang, P.W. Li, S.F. Deng, Humidity sensing properties of $K_{0.5}Na_{0.5}NbO_3$ powder synthesized by metal organic decomposition, Sens. Actuators B 209 (2015) 252–257.

[44] Y. Zhang, X.J. Zheng, T. Zhang, Characterization and humidity sensing properties of $Bi_{0.5}Na_{0.5}TiO_3$-$Bi_{0.5}K_{0.5}TiO_3$ powder synthesized by metal-organic decomposition, Sens. Actuators B 156 (2011) 887–892.
[45] M.J. Lee, H.P. Hong, K.H. Kwon, C.W. Park, N.K. Min, Fast-speed, high-sensitivity polyimide humidity sensors with superhydrophilic carbon nanotube network electrodes, Sens. Actuators B 185 (2013) 97–104.
[46] G.C. Li, L.L. Guan, Y.Q. Liu, C.G. Liu, Template-free solvothermal synthesis of 3D hierarchical nanostructured boehmite assembled by nanosheets, J. Phys. Chem. Solids 73 (2012) 1055–1060.
[47] C. Wu, Z.Y. Wang, Z.Z. Zhi, T.Y. Jiang, J.H. Zhang, S.L. Wang, Development of biodegradable porous starch foam for improving oral delivery of poorly water soluble drugs, Int. J. Pharm. 403 (2011) 162–169.
[48] W.W. Zhang, R.W. Wang, Q. Zhang, J.X. Li, Humidity sensitive properties of K-doped mesoporous silica SBA-15, J. Phys. Chem. Solids 73 (2012) 517–522.
[49] Y.X. Liang, Y.J. Chen, T.H. Wang, Low-resistance gas sensors fabricated from multiwalled carbon nanotubes coated with a thin tin oxide layer, Appl. Phys. Lett. 85 (2004) 666–668.
[50] R. Wang, D. Wang, Y. Zhang, X.J. Zheng, Humidity sensing properties of $Bi_{0.5}(Na_{0.85}K_{0.15})_{0.5}Ti_{0.97}Zr_{0.03}O_3$ microspheres: effect of A and B sites co-substitution, Sens. Actuators B 190 (2014) 305–310.
[51] V. Bondarenka, S. Grebinskij, S. Mickevičius, V. Volkov, G. Zacharova, Thin films of poly-vanadium-molybdenumacid as startingmaterials for humidity sensors, Sens. Actuators B 28 (1995) 227–231.
[52] Q. Qi, T. Zhang, X.J. Zheng, L.F. Wan, Preparation and humidity sensing properties of Fe-doped mesoporous silica SBA-15, Sens. Actuators B 135 (2008) 255–261.
[53] K. Johansen, I. Lundström, B. Liedberg, Sensitivity deviation: instrumental linearity errors that influence concentration analyses and kinetic evaluation of biomolecular interactions, Biosens. Bioelectron. 15 (2000) 503–509.
[54] W.C. Geng, R. Wang, X.T. Li, Y.C. Zou, T. Zhang, J.C. Tu, Y. He, N. Li, Humidity sensitive property of Li-doped mesoporous silica SBA-15, Sens. Actuators B 127 (2007) 323–329.
[55] Q. Qi, T. Zhang, Q.J. Yu, R. Wang, Y. Zeng, L. Liu, H.B. Yang, Properties of humidity sensing ZnO nanorods-base sensor fabricated by screen-printing, Sens. Actuators B 133 (2008) 638–643.
[56] D. Bauskar, B.B. Kale, P. Patil, Synthesis and humidity sensing properties of $ZnSnO_3$ cubic crystallites, Sens. Actuators B 161 (2012) 396–400.
[57] V.K. Tomer, S. Duhan, Nano titania loaded mesoporous silica: Preparation and application as high performance humidity sensor, Sens. Actuators B 220 (2015) 192–200.
[58] J.H. Anderson, G.A. Parks, The electrical conductivity of silica gel in the presence of adsorbed water, J. Phys. Chem. 72 (1968) 3662–3668.
[59] C.D. Feng, S.L. Sun, H. Wang, C.U. Segre, J.R. Stetter, Humidity sensing properties of Nation and sol–gel derived SiO_2/Nafion composite thin films, Sens. Actuators B 40 (1997) 217–222.
[60] E. Quartarone, P. Mustarelli, A. Magistris, M.V. Russo, I. Fratoddi, A. Furlani, Investigations by impedance spectroscopy on the behavior of poly (*N*,*N*-dimethylpropargylamine) as humidity sensor, Solid State Ionics 136–137 (2000) 667–670.
[61] F.M. Ernsberger, The nonconformist ion, J. Am. Ceram. Soc. 11 (1983) 747–750.
[62] G. Casalbore-Miceli, M.J. Yang, N. Camaioni, C.M. Mari, Y. Li, H. Sun, M. Ling, Investigations on the ion transport mechanism in conducting polymer films, Solid State Ionics 131 (2000) 311–321.
[63] S. Liang, X.W. He, F. Wang, W.C. Geng, X. Fu, J. Ren, X.M. Jiang, Highly sensitive humidity sensors based on LiCl–Pebax 2533 composite nanofibers via electrospinning, Sens. Actuators B 208 (2015) 363–368.
[64] K. Jiang, H.R. Zhao, T. Fei, H.M. Dou, T. Zhang, A guest/host composite of $Fe(NO_3)_3$/nanoporous polytriphenylamine assembly for humidity sensor, Sens. Actuators B 222 (2016) 440–446.
[65] Q. Yuan, N. Li, W.C. Geng, Y. Chi, J.C. Tu, X.T. Li, C.L. Shao, Humidity sensing properties of mesoporous iron oxide/silica composite prepared via hydrothermal process, Sens. Actuators B 160 (2011) 334–340.
[66] R. Wang, X.W. Liu, Y. He, Q. Yuan, X.T. Li, G.Y. Lu, T. Zhang, The humidity-sensitive property of MgO-SBA-15 composites in one-pot synthesis, Sens. Actuators B 145 (2010) 386–393.

Biographies

Yong Zhang received his ME degree from the Faculty of Materials, Optoelectronics and Physics, Xiangtan University, China in 2007. He received his PhD in major of materials science and engineering in 2012 from Xiangtan University. Now, he is interested in the field of sensing functional materials, gas sensors and humidity sensors.

Mengjiao Yuan entered the ME course in 2013, and majored in Electronic Science and Technology, Xiangtan University, China.

Bin Jiang entered the ME course in 2013, and majored in Electronic Science and Technology, Xiangtan University, China.

Peiwen Li entered the ME course in 2013, and majored in Electronic Science and Technology, Xiangtan University, China.

Xuejun Zheng received his MS degree in major of structure mechanics in 1989, and PhD degree in the field of fundamental mechanics in 2002 from Xiangtan University. He was appointed a full professor in Faculty of Materials Optoelectronics and Physics, Xiangtan University in 2003. Now, he is interested in the field of sensing functional materials, gas sensors and humidity sensors.